Origin of the voltage hysteresis of MgH_2 electrodes in Li ion batteries

November 26, 2014

D. Meggiolaro[1,2], G. Gigli[1], A. Paolone[2], P. Reale[3], M.L. Doublet[4], S. Brutti[2,5]

[1]Dipartimento di Chimica, Sapienza Università di Roma, 00185 Rome, Italy
[2]Istituto dei Sistemi Complessi, Consiglio Nazionale delle Ricerche (ISC−CNR) UOS Sapienza, 00185 Rome, Italy
[3]ENEA Centro Ricerche Casaccia, via Anguillarese, Cesano (Italy)
[4]Institut Charles Gerhardt, Université Montpellier 2 - Montpellier Cedex 5
[5]Dipartimento di Scienze, Università della Basilicata, 85100 Potenza, Italy

Abstract

Magnesium hydrides is a new and promising anode material for Li-ion cells. Although the reversibility of the conversion reaction of MgH_2 has been experimentally verified, several fundamental aspects of the conversion process in Li cells are still under debate. In this work we report a combined experimental-theoretical study about the origin of voltage hysteresis in the conversion of MgH_2 in lithium cells. Experimentally, the extent of the thermodynamic voltage hysteresis in the first galvanostatic discharge-charge cycle has been determined by the GITT technique and the electrode/electrolyte interface investigated by electrochemical impedance spectroscopy (EIS). Theoretically, the origin of the thermodynamic voltage hysteresis has been evaluated and studied by means density functional theory calculations within the supercell approach. Different elementary reactions have been modelled upon reduction and oxidation on the surfaces of the active phases (i.e. MgH_2, LiH and Mg) and the associated theoretical voltages have been predicted. Experimental and theoretical results have been compared and discussed to draw a comprehensive description of the elementary surface reactions of the MgH_2 conversion in lithium cells.

1 Introduction

Conversion materials are a valuable alternative to intercalation compounds to increase the capacity of next-generation Li-ion cells [1][2]. Contrary to intercalation reactions where a host lattice stands almost unaltered upon the redox incorporation and de-incorporation of lithium ions, a general MX (M=metal, X=F,P,O,H...) material undergoes to a conversion through a complex redox pseudo-displacement reaction with Li^+ to form the reduced metal M and LiX according to the general equation $M_nX_m + nLi^+ + ne^- = nM + Li_nX_m$. As an example, in oxides systems upon reduction, the microstructure of a conversion electrode is drastically altered by forming nanometric metallic particles (3-5 nm) surrounded by an amorphous matrix of Li_2O, while upon oxidation the active material M is generally converted back to M_xO_y in its nanosized form[3][4]. Multi-electron conversion reactions can supply larger specific capacity compared to the typical single electron

insertion-deinsertion reactions. The reversibility of conversion reactions has been verified for various class of compounds (e.g. fluorides, phosphides, oxides, sulphides, hydrides), in particular in nanosized samples whereas bulk systems show only a limited electrochemical activity [5]. Apparently, in nanosized materials the large surface area and the extent of lattice defects enhance the reactivity and the ion mobility through grains interfaces [6].
However upon cycling in lithium cells, even for extremely nanosized conversion materials, a remarkable voltage hysteresis has been always observed between charge and discharge [7]. The magnitude of the hysteresis is proportional to the ionicity of the compound that undergoes the conversion [1]. As discussed by Doublet et al. [7] in the case of phosphides, this voltage hysteresis may have a combined kinetic - thermodynamic origin. In fact, due to the typical insulating character of conversion materials, polarization effects at the electrode are responsible for a large part of the overpotential both in discharge and charge. However thermodynamic components of voltage hysteresis have been highlighted and investigated, both theoretically by density functional theory (DFT) calculations and experimentally by electrochemical techniques such as the galvanostatic intermittent titration test (GITT) [7]. Doublet et al. suggest that the thermodynamic overvoltages is due to different reaction paths occurring on active materials surfaces upon charge or discharge.
Among the various conversion materials one of the most promising and unexplored class of compounds is that of metal hydrides due to their large specific capacity and low voltage hysteresis [1]. Reversible conversion of metal hydrides in a Li cell have been recently reported for MgH_2 [2][8][9][10][11], TiH_2 [12][13] and other hydrides[14][1]. In general, hydrides show the smallest voltage hysteresis among conversion materials: as an example MgH_2 conversion reaction occurs at an average potential of 0.5 V vs Li^+/Li with an apparent voltage hysteresis below 300 mV [2].
In a previous theoretical work about the reactivity of bulk MgH_2 in a conversion reaction with lithium (a) we predicted an electrode potential vs Li^+/Li^0 of 0.55 V, (b) we discarded the possible occurrence of intermediate stoichiometric intercalation compounds upon conversion (i.e. $LiMgH_3$ and Li_2MgH_4), (c) we studied the occurrence of point defects in bulks and nanometric clusters in order to mimic possible elementary step upon conversion [15] and (d) we outlined a possible reaction path in nanosized samples through substitution of Li in the Mg sublattice of MgH_2 with the contemporary breaking of H bonds. Although our study was rigorous thermodynamic investigation of this conversion reaction, the adopted approach was not suitable to provide useful information about the origin of the voltage hysteresis.
In this work we report a combined experimental - theoretical study about the origin of the voltage hysteresis in the conversion of MgH_2 in lithium cells. The magnitude of the voltage hysteresis has been evaluated experimentally by galvanostatic intermittent titration tests (GITT) and the electrode/electrolyte interfaces have been studied by electrochemical impedance spectroscopy (EIS) upon the lithium incorporation and de-incorporation in galvanostatic conditions (GC).
Parallel to the electrochemical characterization, a theoretical investigation of the MgH_2 conversion has been carried out by ab initio density functional theory (DFT) calculations. In order to elucidate the possible thermodynamic origin of the hysteresis in the MgH_2 conversion a comprehensive study of the reactivity of the surfaces of MgH_2, LiH and Mg with Li has been carried out. Several elementary reactions have been modelled on different surfaces for each compound, both in reduction and oxidation, in order to find out the most likely reaction mechanism. Upon reduction, six reactions have been modelled on the (110) and (100) surfaces of MgH_2, whereas upon oxidation four reactions have been modelled on the (100) and (110) surfaces for LiH and (0001) and (100) surfaces for Mg. The cell voltages associated to these reactions have been calculated and compared to experiments.

2 Methods

2.1 Experimental methods

Three electrodes Swagelock-type cells have been assembled in an MBRAUN glove box under dry argon atmosphere with O_2 and H_2O water content below 1 ppm. MgH_2 active material has been prepared following the procedure described in ref. [2]. MgH_2 electrodes have been prepared by cold pressing the mixture of active material (50%) superP carbon (30%) and a polymeric binder (polyvynil difluoride, 20%) onto circular Cu disks (10 mm in diameter) by means of an hand press and a die set. Electrode preparation has been carried out in glove box without exposure to air. Electrodes have been assembled in cells by coupling them with fiberglass Whatman separators and lithium foil counter-electrodes. A lithium reference electrode has been geometrically inserted between the two other electrodes. Merck LP30 electrolyte, constituted by a 1 molar solution of $LiPF_6$ dissolved in an ethylene carbonate and dimethylcarbonate (1:1 in volumes) solvent, has been used.
GITT and CG-EIS combined experiments have been carried out by using a VSP Biologic instrument. During the GITT measurement, a three electrode cell is discharged and charged at a constant current of 100 mAg^{-1}=C/20 for an intermittent τ=7200 s followed by an open circuit relaxation of at least 12 h to reach a steady-state voltage (E_s) that varies upon time less than 1 mVh^{-1}. The latter (E_s) is an approximate measurement of the electron motion force (e.m.f.) of the electrochemical system and it is a good estimate of the thermodynamic working potential of the cell cleaned up from the kinetic polarization effects. The procedure is repeated 10 times with a constant final cut-off voltage of 0.2 V vs. Li.
The GITT test is commonly used in the literature to evaluate the diffusion coefficient of lithium in intercalation electrodes [16]. As already mentioned during the GITT measurement, the three electrode cell is intermittently discharged or charged at a constant current: each titration step is followed by an open circuit relaxation to reach a steady-state voltage (E_s). The change in the steady-state voltage ΔE_s in each titration step is obtained by subtracting the original voltage (E_0, i.e. OCV cell voltage measured at the end of previous rest step at zero current) from the steady-state voltage (E_s, i.e. OCV cell voltage measured at the end of the rest step at zero current).
The process of the chemical diffusion is assumed to obey Fick's second law of diffusion and with a series of simplifications, for sufficient time interval ($\tau \ll L^2/D_{Li^+}$), the equation of D_{Li^+} can be written as:

$$D_{Li^+} = \left(\frac{\Delta E_s}{\Delta E_\tau}\right)^2 \frac{4L^2}{\pi\tau} \tag{1}$$

Being L the thickness of the electrode, and ΔE_τ the voltage jump/drop upon discharge and charge with a non-zero current [16]. The thickness of the electrode L has been evaluated by light optical microscopy before cycling. However, due to the volume expansion of the active material upon lithium incorporation [2], it is expected to increase upon lithium incorporation (see ref [2]) in the conversion reaction of MgH_2. Therefore L has been considered linearly dependent to the lithium content in the electrode ranging from $L(eq_{Li} = 0)$ to $L(eq_{Li} = 1.74) = 1.80\dot{L}(eq_{Li} = 0)$, where $eq_{Li} = 1.74$ is the final lithium loading per MgH_2 formula unit measured at the end of the discharge in the GITT test.
Note that in conversion reactions the effective meaning of the quantity calculated by the Eq.1 is

not straightforward. In fact in conversion electrodes lithium ion diffusion does not occur within the lattice of the active material like in intercalation compounds but likely through grain boundaries. In fact, experimental reports and theoretical studies about the evolution of the electrode micro-morphology suggest that the nucleation and growth of the conversion products form closely packed polycrystalline aggregates where the motion of lithium ions and the other mobile species occurs across binary interphases [17][4][6]. However, besides this qualitative interpretation there is a clear lack of understanding about the dynamics of ions and electrons in conversion electrodes.
In the EIS-CG experiments a galvanostatic discharge-charge rate of C/20=100 mAg^{-1} has been adopted. Five discharge and charge steps of 4h were followed by 1h relaxation and a potentiostatic EIS test at the finally relaxed OCV. The potentiostatic impedance response test has been carried out with a ΔV=5 mV signal in the frequency range 100kHz-1mHz. EIS data have been fitted with equivalent circuits by using the BOUKAMP code [18].

2.2 Theoretical methods

In order to study the mechanism of conversion of MgH_2, a density functional theory study of the elementary reactions occurring on the surfaces of the active phases (i.e. MgH_2, LiH and Mg) has been carried out, both in reduction and oxidation.
The reduction process has been examined through the study of the reactivity of the (110) and (100) surfaces of MgH_2 with Li. To this aim, six different reactions have been modelled: the simple and double adsorption of Li on the MgH_2 surfaces (R1-R1'); the Li adsorption with the contemporary nucleation of Mg (R2); the Li substitution of Mg on its site and the formation of an H vacancy (R3); the formation of a single or double H vacancy on the MgH_2 surfaces (R4-R4').
Upon oxidation four different elementary reactions have been examined: the formation of a single Li vacancy (O1) and the adsorption of Mg with the contemporary double Li vacancies formation on the (100) and (110) surfaces of LiH (O2); the single and double H adsorption on the (0001) and (100) Mg surfaces (O3-O3').
Clean surfaces have been cleaved from the respective relaxed bulk lattices and their thermodynamic stability checked by calculating the respective surface formation energies (SFE) in the supercell approach. The SFE fixes the thermodynamic stability of the different Miller index surfaces and, for stoichiometric surfaces, it is defined as

$$SFE = [E_{slab} - n\mu]/2A \quad (2)$$

where E_{slab} is the energy of the surface, n and μ are respectively the number of formula units in the simulated slab cell and the relative bulk chemical potential and A the area of the modelled surface. Only stoichiometric surfaces have been considered, since non-stoichiometric surfaces (e.g. Mg-terminated MgH_2 (110), Li-terminated LiH (100)) are less stable and likely play a limited role in the thermodynamics of the conversion. A surface chemical potential has been therefore calculated for each phase slab with a specific (hkil) surface and a fixed stoichiometry. This chemical potential has been defined as the DFT energy per formula unit of the calculated phase. Within this approach the surface tension contribution to the thermodynamic stability of each phase for each surface is always taken into account and therefore included in the prediction of the reaction thermodynamics. Elementary reactions have been modelled on one side of the surface slabs in order to avoid images interactions. Several reaction extents have been simulated enlarging the in-plane lattice of the

supercell and dipole corrections have been applied along the direction perpendicular to the slab in order to avoid electrostatic interactions between periodic images. The energetics at 0K have been evaluated for each reaction and the associated thermodynamic voltage ΔV has been calculated according to the general equation

$$\Delta V = -\Delta_r E/nF \tag{3}$$

where $\Delta_r E$ is the total energy of reaction as obtained by the DFT calculations, n the number of exchanged electrons in the reaction and F the Faraday constant. In the expression for $\Delta_r E$ the chemical potential of the species reaching or leaving the surface have been set equal to the surface chemical potentials of the respective species on their most stable surfaces. The chemical potential for Li has been set to the Li bulk value, in order to directly calculate the thermodynamic voltage of the process with respect to the redox couple Li^+/Li^0.
All DFT calculations on surfaces have been carried out in the supercell approach using plane waves basis set (PW) and pseudopotentials as implemented in the VASP code [19]. A gradient corrected exchange correlation functional has been used as formulated by Perdew Burke Enzerhof (PBE) [20] within the projector augmented wave (PAW) method [21]. An energy cutoff of 500 eV on PW's have been imposed for all calculations. Convergence tests on the thickness of the slabs have been performed by increasing the number of atomic layers in the slabs until a constant SFE has been reached for each system. The vacuum thickness between the surface slabs and the number of k points in the Brillouin Zone (BZ) have been converged in order to achieve an accuracy on total energy of about 2 meV/atom. The equilibrium geometry has been obtained by relaxing ions positions until forces on atoms were less than $1x10^{-2}$ eV/Å.

3 Results

3.1 Experimental results

3.1.1 Galvanostatic Intermittent Titration Test

The voltage hysteresis in MgH_2 conversion has been investigated by the GITT experimental technique. In the Fig.1 the lithium loading curve from the GITT test is shown.

The GITT highlights:

1. an average electromotion force (e.m.f.) for the cell of approximately 0.525±0.050 V;

2. an almost constant kinetic polarization along the conversion plateau in discharge of about 103±10 mV that increase monotonically to values $\sim$ 200 mV in the last stages of discharge;

3. a rapidly increasing kinetic polarization upon charge ranging from 40 mV to 500 mV;

4. different equilibrium open circuit voltage (OCV) values in discharge and charge being the mean electrode potentials 0.489±0.050 and 0.560±0.050 V vs Li, respectively

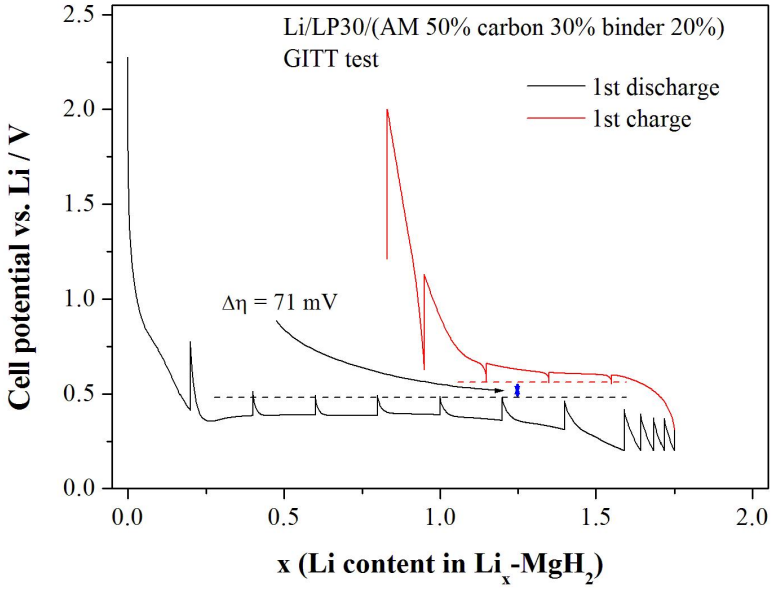

Figure 1: Lithium loading curve vs. cell potential (vs. Li) from a GITT test.

The GITT e.m.f. is, as expected, in good agreement with the experimental average potential between charge and discharge measured by simple GC tests, i.e. 0.5 V vs Li^+/Li^0 [2], and with our theoretical prediction for bulk [15].
The electrode polarization shows different magnitudes and trends upon discharge and charge. In the Fig.2 the evolution of the electrode polarization measured in the GITT experiment is reported versus the lithium content incorporated in the electrode. The electrode kinetic polarization has been calculated as the absolute value of the difference between the last measured cell potential at the end of each galvanostatic step, with a non-zero current, and the steady-state voltage (E_s, i.e. OCV cell voltage measured at the end of the rest step at zero current). An almost constant kinetic polarization along the conversion plateau of about 103±10 mV is observed in discharge, whereas a rapidly increasing kinetic polarization is observed upon charge ranging from 40 mV to 500 mV. Such polarization asymmetry has been already highlighted for conversion materials such as CoP [7].

A thermodynamic voltage hysteresis as large as 71±7 mV is observed between discharge and charge, even after an open circuit voltage relaxation of the cell longer than 12 hours.
This small thermodynamic component accounts for approximately 20-30% of the whole voltage hysteresis observed in standard galvanostatic cycling tests with the same current rate (see ref. [[2]] as an example). It is interesting to observe that at the end of the GITT discharge a decrease of the relaxed OCV is observed. This evidence can be a clue of the onset of alloying of Li into the hcp Mg particles formed upon conversion. In fact this further redox lithium incorporation reaction may occur in conversion MgH_2 electrodes upon discharge at low potentials below 0.3-0.2V, as shown by ex situ X-ray diffraction by Brutti et al. and reported in ref.[2]. Another possible explanation may involve the occurrence of thermodynamic nanosizing effects due to the consumption of the pristine MgH_2 particles [17][4][15].

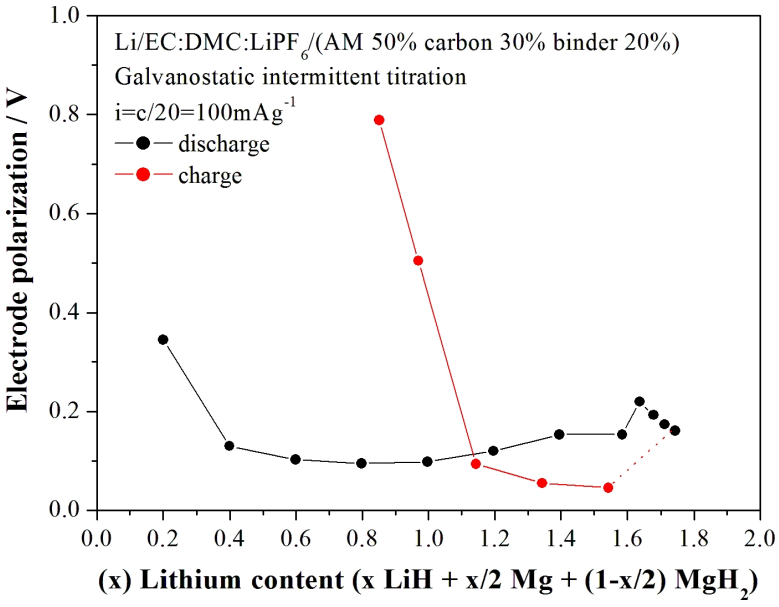

Figure 2: Evolution of the electrode polarization upon lithium incorporation in the GITT experiment

Having in mind the limits of the present understanding of the physical meaning of the quantity calculated from the Eq.1, in the Fig.3 we show the lithium ion diffusion coefficient for the conversion of MgH_2-based electrodes in lithium cells calculated from the GITT voltage data.
The diffusion coefficient smoothly varies upon lithium incorporation. Three different regions can be observed upon discharge:

1. D_{Li^+} decreases monotonically of about 2 orders of magnitude until approximately 1.2 lithium equivalents per MgH_2 molecular formula are incorporated;

2. deeper lithium incorporation (from 1.2 to 1.65 eq per MgH_2) leads to an increase of the diffusion coefficient of more than 1 order of magnitude;

3. in the last stages of discharge it slightly fades.

Upon charge after an increase of about 2 order of magnitudes, the diffusion coefficient follows a trend parallel to the discharge values for similar lithium content. In the last charge step to 2 V vs Li, the diffusion coefficient approximately reaches the value estimated at the beginning of discharge although more than 0.8 eq. Li are still retained in the electrode.

In summary, trends shown in Fig. 3 highlight that lithium ion mobility in the electrode (and/or that of other possible mobile species, i.e. Mg^{2+} and H^-) varies smoothly upon discharge without a simple monotonic slope or abrupt changes. This behaviour is different compared to intercalation compounds where after a typical drop at the beginning of the redox reaction, the lithium diffusion coefficient is almost constant for the whole lithium incorporation/extraction process until a steep decreasing slope is observed in the last stages of the intercalation/deintercalation [16].
One may speculate that the first decreasing trend can be due to the accumulation of Mg and LiH particles over the surface of MgH_2 nanoparticles that in parallel become smaller and smaller. This

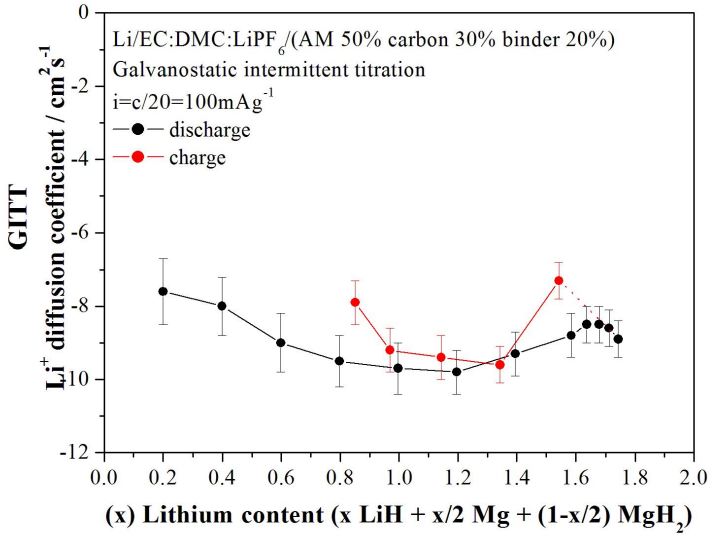

Figure 3: Lithium diffusion coefficient or interphase migration coefficient from the GITT test.

accumulation may lead to an increase of the tortuosity of the lithium microdiffusion path thus increasing the effective length necessary to move ions from the electrode/electrolyte surface to the active MgH_2 particles. On the other hand the increasing trend observed upon discharge for lithium content >1.2 $eq_L i$ per MgH_2 formula unit may be interpreted considering the possible occurrence of fractures across the polycrystalline LiH-Mg-MgH_2 aggregates due to the relevant volume expansions (>50%) at large lithium incorporation. The final decreasing trend in the last stages of discharge may be a clue of the occurrence of the alloying of lithium into the Mg lattice as already observed by us [2].
Turning to Li^+ diffusion coefficient upon lithium extraction, the increase in the first stage of charge may suggest the possible occurrence of a different microdiffusion path of the ions to reach the active surfaces from the electrode/electrolyte interface. This evidence would imply different minimum-energy electroactive solid-solid interfaces (i.e. one among Mg:MgH_2; Mg;LiH; LiH;MgH_2) between the three phases (Mg, LiH, MgH_2) involved in the conversion reaction upon discharge and charge. Similarly to what occurs upon discharge, the following decrease of the diffusion coefficient upon charge may result from the accumulation of the reaction products over the surface of the Mg and LiH particles thus increasing the winding of the charge microdiffusion path. Such speculation requires further support and it is here presented as a simple hypothesis.
In the last part of the charge the increase of the diffusion coefficient to values similar to the beginning of discharge may again be related to the large volume variations (shrinking) upon lithium extraction. In fact a further mechanical stress may newly lead to fractures across the electrode volume.

3.1.2 Electrochemical Impedance Spectroscopy

In order to highlight the changes of the electrolyte/electrode interface upon lithium incorporation and extraction a EIS-CG test has been performed by measuring the impedance spectra of the MgH_2 electrode at various stage of discharge and charge in the first galvanostatic cycle. The collection of

the EIS spectra is shown in the Fig.4.

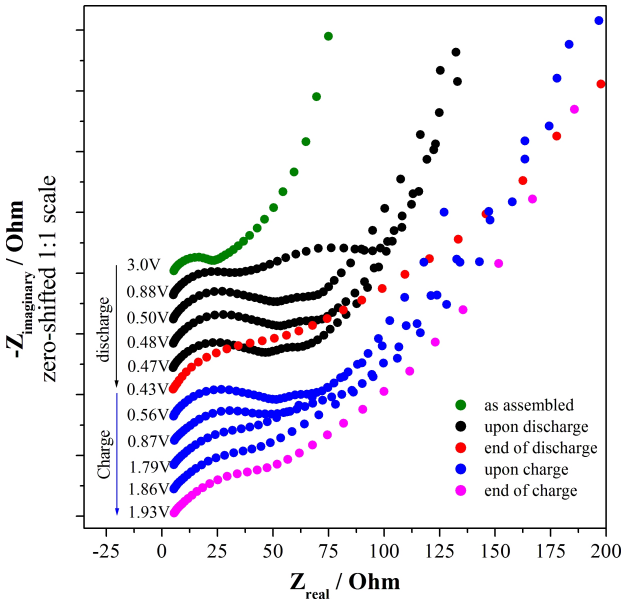

Figure 4: EIS spectra of the MgH_2 electrodes upon lithium incorporation and extraction in a galvanostatic test.

In all EIS spectra upon discharge and charge it is possible to highlight two partially overlapped semi-circles in the high-to-mid frequency range thus suggesting the occurrence of two interfacial processes with shifted time constants [22][23]. These two interfacial processes are likely related to the formation of a passivation film and to a double layer dynamics (charge transfer) [24]. Therefore it is possible to fit this portion of the EIS spectra with an $R_{el}(R_{pf}C_{pf})(R_{ct}C_{dl})$ equivalent circuit, being R_{el}, R_{pf} and R_{ct} the electrolyte, passivation film and charge transfer resistances, respectively, and C_{pf} C_{dl} the capacitances (fitted with two constant phase elements) of the passivation film and the double layer, respectively [23].
On the other hand the electrode impedance response in the low frequency range largely varies upon charge and discharge and it is of complex understanding. It is strongly influenced by the slow motion of the mobile ionic species in the composite electrode [25]. As discussed above (see previous discussion about D_{Li^+} in the GITT results section), such ion dynamics may depend from a number of real phenomena very difficult to model and decouple by EIS (e.g. diffusion through grain boundaries, electrode volume expansion/shrinking, fractures). In fact the fitting of the impedance spectra implies the a priori adoption of an equivalent circuit, leading to a strong bias on the results in all ambiguous cases. In this view here we discuss only the analysis of the high-to-mid frequency range of the EIS spectra. The trend of the resistances of the passivation film and of the charge transfer are shown in the Fig. 5. The resistance of the electrolyte has been omitted in this plot as it does not vary upon discharge/charge.

The small resistance of the passivation film shows a slightly noisy increasing trend upon lithium incorporation and extraction without drastic changes. The formation of the passivation film occurs at 0.8-0.7 V vs Li in the first part of discharge (see figure 1) due to a limited decomposition of the electrolyte. At lower voltage (<0.5V vs Li) the passivation film resistance slightly increase due to a further moderate decomposition of the electrolyte in parallel with the conversion reaction or

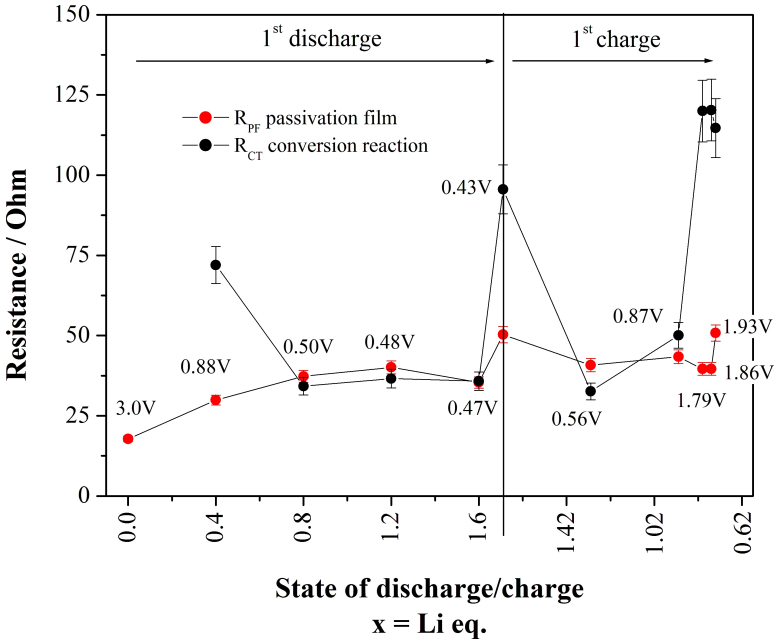

Figure 5: Trend of the resistances of the passivation film and charge transfer upon lithium incorporation and extraction.

by its hardening upon time [26]. Whereas the first stage of the growth of the passivation film is apparently similar to all negative electrode materials [26], the occurrence of the second stage of electrolyte decomposition at lower voltages is less common. A similar behaviour has been already observed in other conversion reaction materials like copper oxide and manganese oxide [5] where a continuous and partially reversible decomposition of the electrolyte has been highlighted by ex situ transmission electron microscopy.
Turning to the charge transfer resistance, it shows very similar drastic changes upon lithium incorporation and extraction. In particular both at the end of discharge and charge the R_{ct} values increase approximately of 150% compared to the voltage plateau ones upon conversion. Both these jumps occur in parallel with a slight increase of the passivation film resistance and the increase of the diffusion coefficient observed in the GITT experiment. Such drastic increase in the R_{ct} value may be interpreted by considering (a) a possible drop in the electron conductivity through the conversion electrode, (b) an increase in the electron transfer resistance from the valence bands of the active material and the conduction band of the carbon additive, (c) a different reaction microkinetics due to the possible competition between the alligation in the Mg lattice and the conversion reaction.

3.2 Theoretical results

3.2.1 The overall conversion reaction (OCR)

In order to model the elementary reactions at the electrode, low Miller index surfaces have been cleaved from the respective bulks. For each phase the two most stable surfaces have been considered: they are reported in Fig. 6 with the relative lattice structures. The modelled surfaces are stoichiometric and the relative SFE's have been calculated according to the Eq. 2 and are reported

System	Surface	SFE(J/m^2)
MgH_2	(110)	0.47
	(100)	0.54
LiH	(100)	0.32
	(110)	0.71
Mg	(0001)	0.54
	(100)	0.63

Table 1: Surface formation energies of the studied surfaces

in the Table 1.

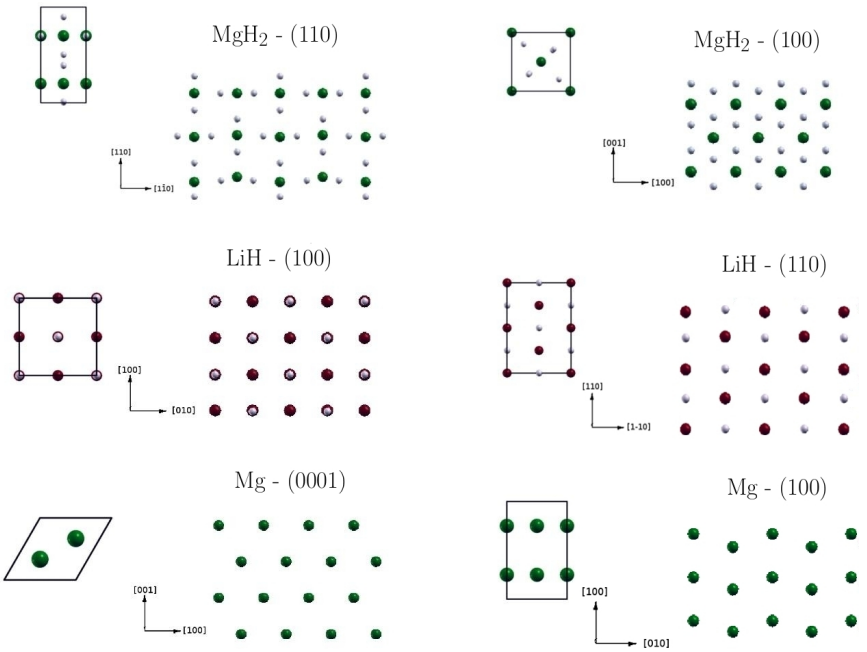

Figure 6: Structures of the modelled surfaces: top and side view

In order to estimate the effect of nanometrization on the energetics of the overall conversion reaction (OCR)

$$2Li^+ + 2e^- + MgH_2 = Mg + 2LiH \ (OCR)$$

the associated thermodynamic voltage has been evaluated according to equation 3, calculating the $\Delta_r E$ term as the difference between the surface chemical potentials of the products and of the reactants in their respective most stable surfaces, i.e. MgH_2(110), LiH (100) and Mg (0001). The as calculated surface chemical potentials of the phases are higher than the respective bulk values due to the surface tension contribution to the energy. For instance, the surface chemical potentials of MgH_2, LiH and Mg in the MgH_2 (110), LiH (100) and Mg (0001) surfaces show an increment with respect to the bulk values of 10 kJ/mol, 5 kJ/mol and 6 kJ/mol respectively. The obtained

voltage for OCR is 0.52 V. This value is slightly lower than the prediction made considering DFT chemical potentials of the bulks, i.e. 0.55 V reported in a previous work by us [15] at the same level of theory. The calculated thermodynamic voltage for the OCR, also incorporating surface effects, (0.52 V) is in excellent agreement with the experimental value, i.e. 0.525±0.005 V, obtained by the GITT technique (see previous section).

3.2.2 Reduction reactions

Upon reduction, six possible elementary reactions between Li and MgH_2 have been modelled on the MgH_2 (110) and (100) surfaces. A pictorial representation of some of these reactions is reported in the Fig.7. A summary of the corresponding predicted thermodynamic potentials (vs Li^+/Li^0) is reported in the Table 2. The coverages values reported in the table (ξ) represent an estimate of the 2D concentration of the lithium ions over the surfaces and have been calculated considering the number of formula units of the respective phase per cell employed in the calculation.

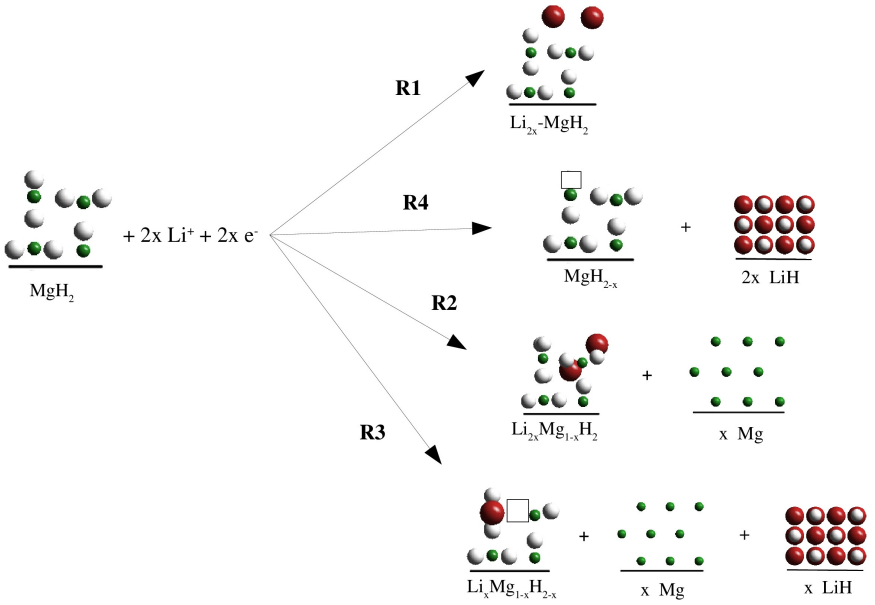

Figure 7: Pictorial representation of modelled reactions upon reduction. They are reported in descending order of spontaneity.

Reactions R1-R1' model the Li adsorption on the MgH_2 surface at different degrees of coverage. The preferential adsorption sites of Li atoms on the surface are in the proximity of H atoms, where weak Li-H bonds are formed with a internuclear distance of about 1.88 and 2.00 Åfor the (100) and (110) surfaces, respectively. The predicted potentials for reactions R1-R1' are negative for all the computed surfaces and for any coverage. Apparently, in the quasi-covalent MgH_2 system a reductive interaction between the Li ion and the active material surface is thermodynamically unfavourable. Reaction R2 models a double Li adsorption with the contemporary formation of a Mg vacancy and the nucleation of metallic Mg surfaces. The extrusion of Mg leads to an asymmetric loss of coordination for the H atoms close to the surface, compensated by the insertion of Li atoms in the slab. The simple formation of a Mg vacancy is energetically unfavourable, both in the bulk and on the surfaces of MgH_2, due to the breaking of two strong partially covalent Mg-H bonds and the

	(110)	(100)
Reaction	ξ (coverage) - Potential (V)	
R1 - xLi + MgH2 = Li_xMgH2		
	(ξ=1/5)	(ξ=2/5)
single Li adsorption	-0.46 V	-0.40 V
R1'- 2xLi + MgH2 = $Li_{2x}MgH2$		
	(ξ=1/10)	(ξ=1/10)
double vicinal Li adsorption	-0.28 V	-0.55 V
	(ξ=1/5)	(ξ=2/5)
	-0.09 V	0.00 V
R2 - 2xLi + MgH_2 = $Li_{2x}Mg_{1-x}H_2$ + x Mg		
	(ξ=1/10)	(ξ=1/10)
double vicinal Li adsorption and Mg nucleation	0.39 V	0.29 V
	(ξ=1/5)	(ξ=2/5)
	0.39 V	0.13 V
R3 - 2xLi + MgH_2 = $Li_xMg_{1-x}H_2$ + x Mg +x LiH		
	(ξ=1/10)	(ξ=1/10)
Li in Mg site and H vacancy formation	0.43 V	0.40 V
	(ξ=1/5)	(ξ=2/5)
	0.46 V	0.54 V
R4 - xLi + MgH_2 = MgH_{2-x} + x LiH		
	(ξ=1/10)	(ξ=1/10)
single H vacancy formation	-0.32 V	-0.36 V
	(ξ=1/5)	
	-0.21 V	
R4' - 2xLi + MgH_2 = MgH_{2-2x} + 2x LiH		
	(ξ=1/10)	(ξ=1/5)
double H vacancy formation	-0.26 V	-0.02 V
	(ξ=1/5)	
	0.14 V	

Table 2: Thermodynamic cell voltage results for elementary discharge reactions at several coverages.

induction of electronic disorder in the system. In reaction R2 this unfavourable thermodynamics is partially counterbalanced by the formation of new Li-H bonds due to the substitutional lithium ions adsorbed on both the (110) and (100) surfaces.
Reaction R3 describes the reductive substitution of a single Mg atom on its lattice site by a single Li^+ ion with a parallel formation of vicinal H vacancy and the contemporary nucleation of Mg and LiH surfaces. In the case of bulk phases, as discussed by us in ref. [15], the Gibbs energy of this reaction is competitive with the OCR. Also in the case of surfaces the predicted potential for this redox reaction at low Li coverages is 0.43 V and 0.40 V on the (110) H-terminated and (100) surface respectively, values very close to the overall conversion cell potential of 0.52 V. At high coverages these values increase and in the case of the (110) surface exceed that of the OCR. It is interesting to observe that all the predicted values for R3 compare well with the relaxed e.m.f. measured by the GITT test upon reduction (i.e. 0.489±0.050 V).
Reactions R4-R4' model the reductive H vacancy formation on the surfaces at different degree of coverage with parallel nucleation of LiH surfaces. Both single H vacancies and vicinal double H vacancies have been modelled. The predicted R4-R4' potentials are negative except for the double vacancy formation on the (110) surface at high coverages. The unfavourable thermodynamics for these processes may be related to resulting electronically disordered MgH_{2-x} system. As expected the double vacancy process R4' is thermodynamically more favoured in comparison to the single vacancy reaction R4, similarly to the case of the bulk phase [15]. This is due to a binding effect between the two vacancies that stabilizes the defective system.
According to all the presented predictions, the most favourite reaction upon reduction is R3 that shows an estimated potential in the range 0.40 – 0.54 V, values comparable with the experimental determination of the thermodynamic e.m.f. upon reduction from the GITT test discussed in the previous section (0.489±0.050 V).

3.2.3 Oxidation reactions

Five different reactions have been modelled upon oxidation from the LiH-Mg system. Similarly to the case of reduction reactions, the corresponding cell potentials have been evaluated. A pictorial representation of the three elementary reactions upon oxidation is shown in the Fig.8 and the corresponding potentials are reported in the Table 3 for different LiH surfaces and coverages.
All the predicted potentials are negative as all processes require electric work to occur. Thus the thermodynamically most favoured processes are those occurring at the smaller voltages in absolute values.

Reaction O1 models the oxidative formation of a Li vacancy in the lattice of LiH. This process is associated to the formation of acceptor states in the electronic structure of LiH and, as in the case of H vacancies in MgH_2, the corresponding thermodynamics is largely unfavourable for both the (100) and (110) surfaces.
Reaction O2 describes the oxidative Mg adsorption on LiH surfaces with a parallel formation of double Li vacancies. The extrusion of Li atoms from the LiH surface occurs with the insertion of the adsorbed Mg atom in the surface slab in order to saturate the lost Li-H bonds. Mg atom in the slab is tetra-coordinated by 4 H vicinal atoms forming weak bonds at a mean distance of 2.88 Å.
The last reactions O3 and O3' have been modelled on the Mg (0001) and (100) surfaces and describe the formation of Mg-H bonds on the Mg surface through the reaction of the latter with LiH. Single H adsorption is more unfavorable with respect to the vicinal double adsorption: in both cases the

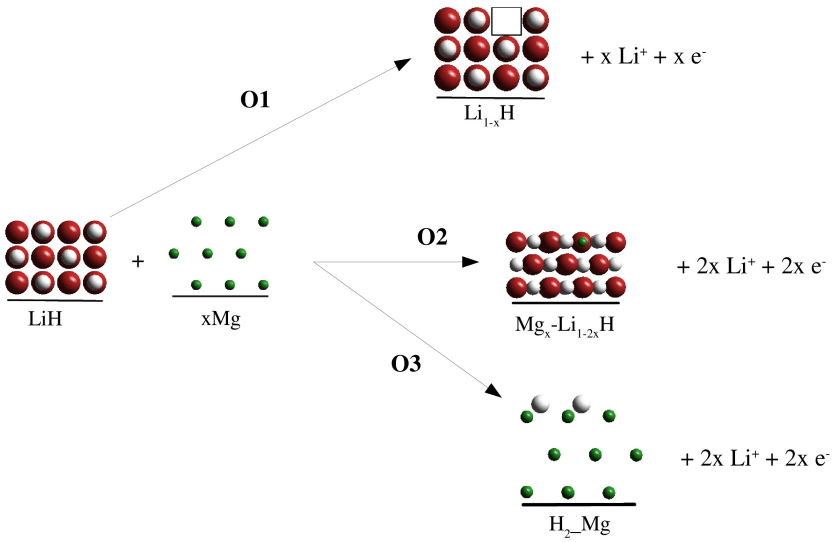

Figure 8: Pictorial representation of modelled reactions upon oxidation in descending order of spontaneity.

H adsorption leads to the formation of a Mg-H bond of length 2.04 Å, very close to the bulk bond length of MgH_2 (1.92 Å). The analysis of the thermodynamic potential associated to this reaction highlights that this reaction is the most favourable surface process among all the studied systems upon oxidation with a voltage of 0.58 V. According to the presented predictions, the most favourite reaction upon oxidation is O3' that shows an estimated potential in the range 0.58 – 0.66 V, values comparable with the experimental determination of the thermodynamic e.m.f. upon oxidation from the GITT test discussed in the previous section (0.560±0.050 V).

4 Discussion

The voltage hysteresis observed in MgH_2-based electrodes in Li cells can be split in two components: one kinetic and one thermodynamic. Starting from the kinetic component, the trend of the voltage polarization upon conversion shown in the Fig. 2 highlights an almost constant value upon discharge and a rapidly increasing slope upon charge. In parallel, the estimated diffusion coefficients of the ionic mobile species upon lithium incorporation (see Fig. 3) show larger variations of more than 2 orders of magnitude. This asymmetry suggests a weak correlation between the variation of the ionic mobility within the electrode and the increase of the kinetic cell polarization. A closer correlation can be found between the kinetic polarization and the trend of the charge transfer resistance measured by EIS (see Fig. 5) upon lithium incorporation. In fact the increase of the electrode polarization occurs in parallel with the increase of the charge transfer resistance. Being the charge transfer resistance measured by EIS affected by variation of both ionic and electrode mobility in the electrode [27], these experimental evidences suggests that the kinetic polarization in MgH_2 based electrodes are likely related to variation of the overall electrode conductivity and/or an increase in the electron transfer resistance from the valence bands of the electroactive material and the conduction band of the carbon additive.
Turning to the thermodynamic overvoltages, our DFT predictions suggest that two different reac-

	LiH (110)	LiH (100)
Reaction	ξ (coverage) - Potential (V)	
O1 - LiH = $Li_{1-x}H$ + x Li		
	(ξ=1/8)	(ξ=1/8)
Li vacancy formation	-3.26 V	-2.77 V
	(ξ=1/32)	(ξ=1/32)
	-3.09 V	-2.46 V
O2 - LiH + Mg = $Mg_xLi_{1-2x}H$ + 2x Li		
	(ξ=1/8)	(ξ=1/8)
Mg adsorption and double Li vacancy formation	-0.78 V	-1.10 V
	(ξ=1/32)	(ξ=1/32)
	-0.77 V	-0.74 V
	Mg(0001)	Mg(100)
O3 - xLiH + Mg = MgH_x + x Li		
	(ξ=1/4)	(ξ=1/4)
single H adsorption on Mg	-1.22 V	-0.71 V
O3' - 2xLiH + Mg = MgH_{2x} + 2x Li		
	(ξ=1/4)	(ξ=1/4)
double H adsorption	-0.58 V	-0.66 V

Table 3: Thermodynamic cell voltage results for the charging reactions at different coverages

tion paths occur upon discharge and charge driven by difference redox chemistry on surfaces. In particular, upon discharge, our DFT calculations find as the most favored reaction the reductive substitution of surface Mg atoms by Li in the MgH_2 lattice (with the parallel formation of a H-vacancy): it is predicted to occur at approximately 0.46 $\pm$0.06 V in very good agreement with the experimental cell e.f.m. upon discharge of 0.489 $\pm$ 0.050 V.
On the other hand upon charge our computational investigation suggests that the most favored process is the double H-shift from the LiH to Mg surfaces. This reaction is predicted to occur at 0.62 $\pm$ 0.04 V in agreement within the errors with the experimental cell e.f.m. upon charge of 0.560 $\pm$0.050 V.
The sum of the thermodynamic overvoltages upon discharge and charge give a predicted thermodynamic voltage hysteresis of 0.16 V in satisfactory agreement the experimental value of approximately 0.071 V obtained from the GITT test.
The asymmetric redox reactivity upon discharge and charge has been already highlighted by Doublet et al. [7] in the case of CoP conversion reaction. Such behaviour is not necessarily surprising since the two active materials upon discharge and charge, i.e. MgH_2 and Mg, are very different, both structurally and from the point of view of electronic structure. In particular MgH_2 is an insulator with a band gap of 5.6 eV [28][29], whereas Mg is a metal. In this view, starting from our DFT analysis, some additional speculations about the reaction mechanism can be drawn.
In order to evaluate the redox properties of the pristine electroactive materials upon reduction and oxidation, the Fukui functions of MgH_2 (110) and Mg (0001) surfaces have been studied. In particular the response of the MgH_2 system to the electron addition and of the Mg system to

the electron removal have been considered. The Fukui function is the real space plot of the difference of the electronic charge density between a neutral and a charged modelled system and is extensively used in quantum chemistry in order to identify the sites of electrophilic or nucleophilic attack in a molecule [30]. The Fukui functions for Mg and MgH_2 have been defined respectively as $F^-_{Mg} = \rho^{N-\epsilon}_{Mg}(\mathbf{r}) - \rho^N_{Mg}(\mathbf{r})$ and $F^+_{MgH_2} = \rho^{N+\epsilon}_{MgH_2}(\mathbf{r}) - \rho^N_{MgH_2}(\mathbf{r})$, where the charge density difference $F^\pm$ is evaluated on the real space FFT grid between the density $\rho^{N\pm\epsilon}$ of the system with $N \pm \epsilon$ electrons and the neutral ground state density ρ^N. Only limited fractions of charge ϵ have been added and subtracted to the MgH_2 and Mg systems respectively, in order to avoid large alteration of the electronic structure of the systems with respect to the ground states. Fukui functions plots are reported in the Fig. 9 for MgH_2 and Mg slabs.

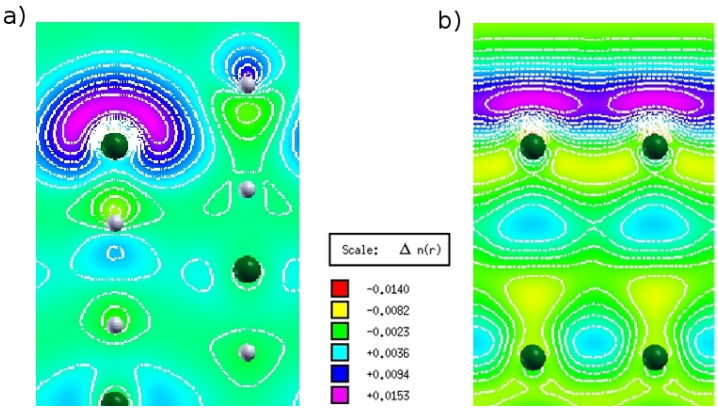

Figure 9: Calculated Fukui functions for MgH_2 (110) (a) and Mg (0001) (b).

The Fukui functions for both MgH_2 and Mg surfaces are localized in the first layers of the slabs, highlighting a dominant role of the surface states with respect to the bulk states in the redox processes.

In the case of MgH_2 (Fig. 9a) the added charge localizes in the proximity of the Mg atom placed on the surface, although a sensible charge amount can be trapped by the H atoms saturating the surface. A more detailed analysis of the Fukui function results for MgH_2 can be drawn by the electronic band structure of the surface. As generally reported [30], the Fukui functions F^+ and F^- can be approximated by the lowest unoccupied molecular orbital (LUMO) and highest occupied molecular orbital (HOMO) charge densities respectively, i.e. $F^+(\mathbf{r}) \approx \rho_{LUMO}(\mathbf{r})$ and $F^-(\mathbf{r}) \approx \rho_{HOMO}(\mathbf{r})$. In Fig. 10 the surface projected electronic band structure of the (110) H-terminated surface of MgH_2 is reported along the M-X' direction in the BZ.

The occurrence of the electronic surface states within the band edge is nicely evident by comparing the projected electronic states of the bulk into the surface BZ with the band structure of the MgH_2 surface. The lowest unoccupied states, i.e. LUMO, are represented by the surface states at the bottom of the conduction band near the high symmetry point M. The plot in real space of the corresponding Kohn-Sham orbital highlights the localization of the LUMO on the Mg atom at the top of the surface, with an excellent resemblance with the plot of the Fukui function. Furthermore, the analysis of the pdos (here not reported) reveals the cationic character of the surface band at the bottom of the conduction band due to unoccupied states on the Mg surface atoms.

In the case of the Mg a charge depletion at the top of the surface is localized in proximity of the outer Mg atoms. Contrary to the MgH_2 (110) case, here a direct interpretation of the Fukui

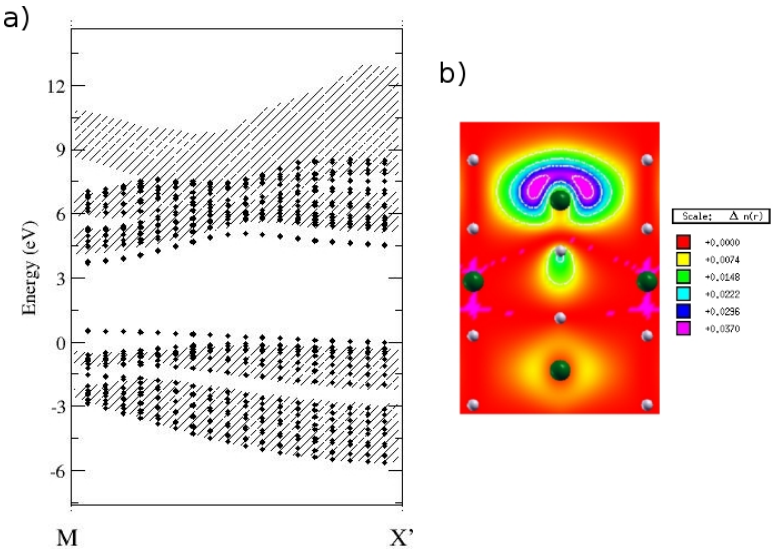

Figure 10: (a) Surface projected electronic band structure of MgH_2 (110) along the M-X' line in BZ; (b) Plot of the LUMO Kohn-Sham orbital at M.

Reaction	atoms	BC reagents	BC product	BC reference
R3 on (100)	Mg	6.37	6.35	
	H	1.82	1.83	1.84 - LiH (100)
	Li	3.00	2.17	2.15 - LiH (100)
O3' on (0001)	Mg	8.00	6.37	6.37 - MgH_2(110)
	H	1.00	1.98	1.82 - MgH_2(110)

Table 4: Bader charges analysis for reactions R3 and O3'

functions in terms of frontier orbitals is not straightforward, due to the ambiguous nature of the smeared orbitals at the Fermi level of a metal.
In Tab. 4, the Bader charges (BC) for the most thermodynamically favourite reaction upon reduction and oxidation (i.e. R3, O3') are reported.

Upon reduction, reaction R3 models the substitution of Mg by a Li ion with the contemporary nucleation of Mg and a non stoichiometric nucleation of LiH as distinct phases. As reported in the Tab. 4, upon reaction R3 the BC of Li ion decrease from a value of 3.00 to 2.17, a value close to that of Li in the LiH phase. This may be a seed of an incipient nucleation of the LiH phase directly on the MgH_2 surface. In fact, the Li-H bond formed on the surface has a mean bond lengths of 1.73 Å, a value similar to the mean distances in the LiH phase (i.e. 2.03 Å). BC of Mg and H atoms does not show sensible alterations.
Upon oxidation the most favourite process is reaction O3', i.e. the adsorption of two H atoms on the surfaces of metallic Mg with the contemporary release of two Li^+ ions in the electrolyte. This process can be described in terms of a nucleation of layers of the MgH_2 phase on the surface of Mg (0001). In fact, after the adsorption, the BC's of the Mg atoms on the surface close to the hydrogens show a marked decrease, passing from the 7.93e to 6.37e, a value almost identical to the

BC calculated for the MgH_2-(110) surface.
The layers projected density of states (LPDOS) for the O3' reaction product is reported in the Fig. 11.

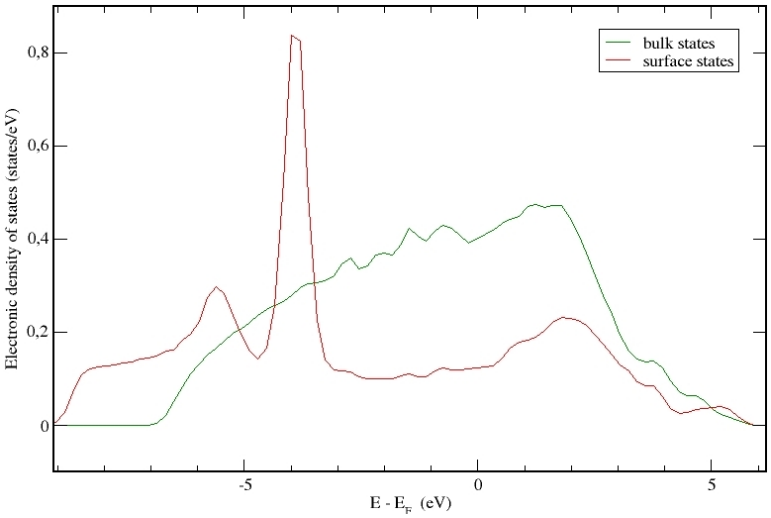

Figure 11: Layers projected density of states for the product of reaction O3', i.e. H adsorbed Mg (0001) surface.

The LPDOS projected on the s and p orbitals of the Mg atoms on the surface together with the therein adsorbed hydrogens (surface states) highlights the opening of a band gap whereas bulk states still predict the metallic character of the Mg inner slab layers (bulk states). This difference implies the formation of a passivating and insulating H-layer on the Mg (0001) surface upon reaction O3'. These hydrogens ad-layer on the Mg surface may be a possible explanation for both the increasing voltage polarization upon oxidation observed in the GITT experiment and the parallel increasing trend of the R_{ct} measured by EIS upon charge. In fact, the insulating character of the passivating H-layer likely leads to a cumulative increase of the electron transfer resistance from the Fermi level of the Mg bulk states to the H-saturated surfaces (and then to the carbon conductive additive) thus making more and more difficult the extraction of electrons upon charge.

5 Conclusions

The study about the origin of the voltage hysteresis in the conversion reaction of MgH_2 has been carried out by a combined experimental-theoretical approach. The two contributions (i.e. thermodynamic and kinetic) to the voltage hysteresis of MgH_2 have been investigated and discussed in the light of the results of the electrochemical GITT and EIS tests and DFT calculations.
The kinetic polarization of the MgH_2 electrodes is strongly affected by the electron conduction through the electrode and/or by the electron transfer resistance from the carbon additive to the surface of the electroactive specie.
A thermodynamic overvoltage of 71 mV between charge and discharge has been measured by the GITT test, confirming the limited extent of the hysteresis in non ionic compounds. Results from the GITT experiments agree very well with the results of the DFT calculations. In particular, within

DFT calculations a value of 0.14 V for the thermodynamic overvoltage has been found considering a different redox reaction path between discharge and charge, i.e. reactions R3 and O3'.

References

[1] A.; Nazri G. A.; Tarascon J. M.; Aymard L. Oumellal, Y.; Rougier. *Nature Materials*, 7(7):916, 2008.

[2] S. Brutti; G. Mulas; E. Piciollo; S. Panero; P. Reale. *J. Mater. Chem*, 22:14531, 2012.

[3] T.R.Kuykendall S.Aloni S.Xun E.Lin V.Battaglia Y.Zhang L.Ji, Z.Tan. *Phys Chem Chem Phys*, 13:7170, 2011.

[4] M.-L. Doublet A.L. Dalverny, J.-S.Filhol. *J.Mater.Chem.*, 21:10134, 2011.

[5] D.Larcher-M.R.Palacin J.Cabana, L.Monconduit. *Adv. Mater.*, 22:E170, 2010.

[6] M.-H.Chen-L.Wu N.Pereira K.Thornton A.Van der Ven Y.Zhu G.G.Amatucci J.Graetz F.Wang, H.-C.Yu. *Nat.Commun.*, 3:1201, 2012.

[7] R. Khatib; A.L. Dalverny; M. Saubanère; M. Gaberscek; M.L. Doublet. *J. Phys. Chem. C*, 117:837–849, 2013.

[8] A.Rougier G.A.Nazri L.Aymard Oumellal, M.Courty. *Int.J.Hydrogen En.*, 39:5852, 2014.

[9] S.Bastide C.Cachet-Vivier E.Leonel S.Sengmany E.Leroy L.Aymard J.-P.Bonnet M.Latroche Y.Oumellal, C.Zlotea. *Nanoscale*, 6:14459, 2014.

[10] J.-P.Bonnet-J.Zhang F.Cuevas M.Latroche J.-L.Bobet L.Aymard W.Zaidi, Y.Oumellal. *J.Power Sources*, 196:2854, 2011.

[11] K.Kawahito-K.Hirabayashi-H.Miyaoka Y.Kojima S.Ikeda, T.Ichikawa. *Chem. Common.*, 49:71741, 2013.

[12] Y. Oumellal et al. *International Journal of Hydrogen Energy*, 37:7831.7835, 2012.

[13] J.-M.Tarascon-L.Aymard Y.Oumellal, A.Rougier. *J.Power Sources*, 192:698, 2009.

[14] J.-P.Bonnet-F.Cuevas M.Latroche J.Zhang J.-L.Bobet A.Rougier-L.Aymard Y.Oumellal, W.Zaidi. *Int.J.Hydrogen En.*, 37:7831, 2012.

[15] D. Meggiolaro; G. Gigli; A. Paolone; F. Vitucci; S. Brutti. *Journal of physical chemistry C*, 117:22467−22477, 2013.

[16] J.Shu S.Gao L.Chen L.feng Y.Ren. 2013 36 495 W.Zheng, M.Shui. *Bull.Mater.Sci.*, 36:495, 2013.

[17] A.Van der Ven K.Thornton N.Pereira Y.Zhu G.G.Amatucci-J.Graetz [F.Wang, H.-C.Yu. *ECS Transaction*, 50:19, 2012.

[18] B.A. Boukamp. *Solid State Ionics*, 18-19:136–140, 1986.

[19] G. Kresse; J. Furthmuller. *Comput. Mater. Sci.*, 6:15, 1996.

[20] J. P. Perdew; K. Burke; and M. Ernzerhof. *Phys. Rev. Lett.*, 77:3865, 1996.

[21] P. E. Blochl. *Phys. Rev. B*, 50:17593, 1994.

[22] D. Aurbach M.D. Levi. *J. Phys. Chem. B*, 101:4630, 1997.

[23] D. Aurbach M.D. Levi. *J. Phys. Chem. B*, 101:4641, 1997.

[24] D. Aurbach M.D. Levi. *Electrochimica Acta*, 45:167, 1999.

[25] D. Aurbach M.D. Levi. *J. Phys. Chem.*, 108:11693, 2004.

[26] P. Maire e P. Novak P. Verma. *Electrochimica Acta*, 55:6332, 2010.

[27] Ho Jang Chee Burm Shin Won Il Cho. Bull Seung Ho Yu, Chang Kyoo Park. *Korean Chem. Soc.*, 32:852, 2011.

[28] H. Arwin R. Griessen I.A. Isidorsson, I.A.M.E. Giebels. *Phys. Rev. B*, 68:115112, 2003.

[29] G.A. de Wijs G. Brocks M.J. van Setten, V.A. Popa. *Phys. Rev. B*, 75:35204, 2007.

[30] P.K. Chattaraj. *Chemical Reactivity Theory: A Density Functional View*. CRC Press, 2009.